Dynamic clamping human and rabbit atrial calcium current: narrowing I_{CaL} window abolishes early afterdepolarizations

Sarah Kettlewell[1], Priyanka Saxena[1], John Dempster[2], Michael A. Colman[3] (iD), Rachel C. Myles[1] (iD), Godfrey L. Smith[1] and Antony J. Workman[1] (iD)

[1] *Institute of Cardiovascular & Medical Sciences, University of Glasgow, Glasgow, UK*
[2] *Strathclyde Institute of Pharmacy & Biomedical Sciences, University of Strathclyde, Glasgow, UK*
[3] *School of Biomedical Sciences, University of Leeds, Leeds, UK*

Edited by: Don Bers & Robert Harvey

Key points

- Early-afterdepolarizations (EADs) are abnormal action potential oscillations and a known cause of cardiac arrhythmias. Ventricular EADs involve reactivation of a Ca^{2+} current (I_{CaL}) in its 'window region' voltage range. However, electrical mechanisms of atrial EADs, a potential cause of atrial fibrillation, are poorly understood.
- Atrial cells were obtained from consenting patients undergoing heart surgery, as well as from rabbits. I_{CaL} was blocked with nifedipine and then a hybrid patch clamp/mathematical-modelling technique, 'dynamic clamping', was used to record action potentials at the same time as injecting an artificial, modifiable, I_{CaL} ($I_{CaL,D-C}$).
- Progressively widening the $I_{CaL,D-C}$ window region produced EADs of various types, dependent on window width. EAD production was strongest upon moving the activation (*vs.* inactivation) side of the window.
- EADs were then induced by a different method: increasing $I_{CaL,D-C}$ amplitude and/or K^+ channel-blockade (4-aminopyridine). Narrowing of the $I_{CaL,D-C}$ window by ∼10 mV abolished these EADs.
- Atrial I_{CaL} window narrowing is worthy of further testing as a potential anti-atrial fibrillation drug mechanism.

Abstract Atrial early-afterdepolarizations (EADs) may contribute to atrial fibrillation (AF), perhaps involving reactivation of L-type Ca^{2+} current (I_{CaL}) in its window region voltage range. The present study aimed (i) to validate the dynamic clamp technique for modifying the I_{CaL} contribution to atrial action potential (AP) waveform; (ii) to investigate the effects of widening the window I_{CaL} on EAD-propensity; and (iii) to test whether EADs from increased I_{CaL} and AP duration are supressed by narrowing the window I_{CaL}. I_{CaL} and APs were recorded from rabbit and human atrial myocytes by whole-cell-patch clamp. During AP recording, I_{CaL} was inhibited (3 μM nifedipine) and replaced by a dynamic clamp model current, $I_{CaL,D-C}$ (tuned to native I_{CaL} characteristics), computed in real-time (every 50 μs) based on myocyte membrane potential. $I_{CaL,D-C}$-injection restored the nifedipine-suppressed AP plateau. Widening the window $I_{CaL,D-C}$, symmetrically by stepwise simultaneous equal shifts of half-voltages ($V_{0.5}$) of $I_{CaL,D-C}$ activation (negatively) and inactivation (positively), generated EADs (single, multiple or preceding repolarization failure) in a window width-dependent manner, as well as AP alternans. A stronger EAD-generating effect resulted from independently shifting activation $V_{0.5}$ (asymmetrical widening) than inactivation $V_{0.5}$; for example, a 15 mV activation shift produced

EADs in nine of 17 (53%) human atrial myocytes *vs.* 0 of 18 from inactivation shift ($P < 0.05$). In 11 rabbit atrial myocytes in which EADs were generated either by increasing the conductance of normal window width $I_{CaL,D-C}$ or subsequent 4-aminopyridine (2 mM), window $I_{CaL,D-C}$ narrowing (10 mV) abolished EADs of all types ($P < 0.05$). The present study validated the dynamic clamp for I_{CaL}, which is novel in atrial cardiomyocytes, and showed that EADs of various types are generated by widening (particularly asymmetrically) the window I_{CaL}, as well as abolished by narrowing it. Window I_{CaL} narrowing is a potential therapeutic mechanism worth pursuing in the search for improved anti-AF drugs.

Corresponding author A. J. Workman: Institute of Cardiovascular & Medical Sciences, College of Medical, Veterinary & Life Sciences, University of Glasgow, 126 University Place, Glasgow G12 8TA, UK.   Email: antony.workman@glasgow.ac.uk

Introduction

Afterdepolarizations are premature action potentials (AP) or subthreshold depolarizations that depend on the preceding AP for their formation (Fozzard, 1992). Early afterdepolarizations (EAD) are transient reversals of AP repolarization that occur either during early (phase 2 EADs) or terminal (late phase 3 EADs) repolarization (Weiss *et al.* 2010). EADs can promote arrhythmias by causing either triggered activity, or electrical heterogeneity which could predispose to unidirectional conduction block and reentrant excitation (Wit & Boyden, 2007; Weiss *et al.* 2010; Colman *et al.* 2017), and they are an established cause of polymorphic ventricular tachycardia in long QT syndrome (Yan *et al.* 2001). Evidence is accumulating that EADs could also be involved in the generation and maintenance of the most common cardiac arrhythmia: atrial fibrillation (AF) (Burashnikov & Antzelevitch, 2003; Wit & Boyden, 2007; Guo *et al.* 2010; Watanabe *et al.* 2010; Numata *et al.* 2012). There is a major unmet clinical need to develop more effective and safe anti-AF drugs with novel mechanisms of action (Workman *et al.* 2011). Because the suppression of atrial EADs may be a potential therapeutic target, investigations aimed at improving our understanding of the electrophysiological mechanisms of their formation and termination are required.

The dynamic clamp, a powerful hybrid patch clamp/computational modelling technique, is emerging as a tool ideally suited to such investigations (Wilders, 2006; Berecki *et al.* 2014; Ortega *et al.* 2018). EADs result from a complex interaction between membrane voltage (V_m), ion currents, such as L-type Ca^{2+} (I_{CaL}), Na^+/Ca^{2+}-exchanger ($I_{Na/Ca}$), late Na^+ (I_{NaL}) and delayed rectifier (I_{Ks}, I_{Kr}), and intracellular Ca^{2+} (Ca^{2+}_i)-cycling, although it is exceedingly difficult to dissect these components and study them systematically (Weiss *et al.* 2010; Qu *et al.* 2013). Regenerative reactivation of I_{CaL} in the 'window region' (where steady-state I_{CaL} activation and inactivation curves overlap), when AP duration (APD) is sufficiently prolonged, is considered a prominent EAD mechanism,

as shown in the ventricle (January & Riddle, 1989; Fozzard, 1992; Weiss *et al.* 2010; Qu *et al.* 2013). Dynamic clamping, by injecting into cardiomyocytes a mathematically modelled I_{CaL} that changes dynamically according to V_m, permits the investigation of effects on APs and EADs of systematically manipulating the voltage-dependent characteristics of this window current. Furthermore, because the injected current is not carried by Ca^{2+} ions, this provides a unique opportunity to attempt to separate the electrical effects of I_{CaL} from the chemical effects of Ca^{2+} (Berecki *et al.* 2014). Dynamic clamping has been used, in rabbit ventricular myocytes, to show that EADs produced by H_2O_2 or low $[K^+]_o$ could be suppressed purely by the electrical effect of either shifting I_{CaL} activation or inactivation curves to narrow the window region (Madhvani *et al.* 2011), or decreasing a non-inactivating, pedestal component of I_{CaL} (Madhvani *et al.* 2015). Furthermore, a mathematical model of AP that was optimized after dynamic clamping several ion currents in guinea-pig ventricular myocytes showed that, when APD was sufficiently prolonged, an increase in I_{CaL} conductance could produce EADs suggestive of window I_{CaL} reactivation (Devenyi *et al.* 2017).

However, in contrast to ventricle, little is known about the contribution of window I_{CaL} to EAD formation in the atrium and, to our knowledge, no study has yet dynamic clamped I_{CaL} in atrial myocytes from any species. In rabbit atrial myocytes, we previously observed that the take-off potential of EADs (produced by decreasing transient outward K^+ current (I_{TO}) in the presence of β-adrenergic stimulation) was consistently close to the V_m of the I_{CaL} window centre (Workman *et al.* 2012). This suggested that atrial EADs could also involve reactivation of window I_{CaL}. However, whether the propensity to EADs, in either rabbit or human atrial myocytes, could be altered by shifting either I_{CaL} voltage-dependent activation or inactivation, presently remains unknown. Such knowledge would advance our mechanistic understanding of atrial EAD formation and could have a crucial bearing on the potential clinical therapeutic utility of

window I_{CaL} modification in the treatment of AF. Because the atria of patients with established (chronic) AF have a shortened APD and reduced I_{CaL}, having undergone electrical remodelling (Workman *et al.* 2008; Heijman *et al.* 2014), this could limit the therapeutic potential of window I_{CaL} modification in such patients. However, such a limitation should not be expected in patients with non-AF-remodelled atria but who are nevertheless susceptible to new-onset or paroxysmal AF.

The present study aimed to: (i) validate the dynamic clamp for simulating, in atrial myocytes from rabbits and from patients in sinus rhythm, the electrical contribution of I_{CaL} to APs; (ii) investigate the effects of widening the I_{CaL} window (symmetrically and asymmetrically) on the propensity to induce EADs; and (iii) test whether EADs produced by increasing the I_{CaL} conductance and APD, could be supressed by narrowing the I_{CaL} window.

Methods

Ethical approval

Procedures and experiments involving human atrial cells were approved by West of Scotland Research Ethics Service (REC: 99MC002, 17/WS/0134). Written, informed consent was obtained from all patients. The investigation conformed with the principles outlined in the *Declaration of Helsinki*. Procedures and experiments involving rabbit atrial cells (UK Project Licences: 60/4206, 70/8835) were approved by Glasgow University Ethics Review Committee, and conformed with the guidelines from Directive 2010/63/EU of the European Parliament on the protection of animals used for scientific purposes. The investigators understand the ethical principles under which the *Journal of Physiology* operates, and our work complies with the animal ethics checklist in (Grundy, 2015).

Atrial cardiomyocytes

Cardiomyocytes were isolated from rabbit and human atrial tissues, as described previously (Workman *et al.* 2000; Workman *et al.* 2001). Rabbits (New Zealand White [Envigo, Huntington, UK], male, aged 16–34 weeks, weighing 2.1–3.6 kg, feeding *ad libitum*; $n = 36$) were humanely killed by I.V. injection of anaesthetic (100 mg kg^{-1} Na$^+$-pentobarbital, via the left marginal ear vein) and removal of the heart, which was retrogradely perfused via the aorta for enzymatic dissociation of left atrial cells (Workman *et al.* 2000). Right atrial tissues were obtained from 28 adult patients (66 $\pm$ 2 years; 20 male, eight female) undergoing cardiac surgery (82% coronary artery bypass graft, 36% aortic valve replacement). All patients were in sinus rhythm on

the day of surgery. One patient had a history of paroxysmal AF; none had chronic AF; 75% had angina, 59% had hypertension, 21% had myocardial infarction and 15% had diabetes. Left ventricular ejection fraction was 61 $\pm$ 2% (including two patients <45%). Cardiac drugs: β-blocker (79%), angiotensin-converting enzyme inhibitor/angiotensin receptor-blocker (39%), Ca^{2+} channel-blocker (CCB) (29%), statin (79%), nitrate (50%), nicorandil (14%) and eplerenone (4%). Cardiomyocytes were isolated by the 'chunk' method (Workman *et al.* 2001), stored ($\leq$9 h, $\sim$20 °C) in cardioplaegic solution (mM): 70 KOH, 40 KCl, 50 L-glutamic acid, 20 taurine, 20 KH$_2$PO$_4$, 3 MgCl$_2$, 10 glucose, 10 Hepes and 0.5 EGTA (pH 7.2).

Whole-cell-patch clamp

Cardiomyocytes were superfused (35–37 °C) with a physiological salt solution (mM): 140 NaCl, 4 KCl, 1.8 CaCl$_2$, 1 MgCl$_2$, 11 glucose and 10 Hepes (pH 7.4). Microelectrodes contained (mM): 130 K-aspartate, 15 KCl, 10 NaCl, 1 MgCl$_2$, 10 Hepes and 0.1 K$_2$EGTA (pH 7.25). The resulting liquid–liquid junction potential (+9 mV; bath relative to pipette) was compensated for *a priori* (Neher, 1992). Microelectrode resistances were $\sim$3–6 MΩ. Associated voltage errors during peak I_{CaL} recording were minimized by bridge-balancing prior to sealing and expected to be <5 mV; no subsequent series resistance compensation was applied. Membrane currents and APs were stimulated and recorded by whole-cell-patch clamp, with an AxoClamp 2B amplifier (Axon Instruments, Foster City, CA, USA) and WinWCP (J. Dempster, University of Strathclyde, Glasgow, UK) or Clampex (Axon Instruments) software. Ruptured (rather than perforated) patch configuration was chosen for its relative ease of controlling access resistance and because preservation of I_{CaL}-associated intracellular signalling was not required when dynamic clamping (when I_{CaL} was necessarily inhibited). I_{CaL} was stimulated with 300 ms voltage pulses (Fig. 2*A*). Pulse frequency was 1 Hz, for best approximation of the influence of Ca^{2+}-induced inactivation of I_{CaL} in the model I_{CaL} when dynamic clamping APs at similar rates. Contaminating currents were suppressed by 4-aminopyridine (4-AP; 5 mM), niflumic acid (0.1 mM) and TTX (5 µM). APs were recorded under current clamp in bridge-mode, stimulated continuously with pulses of 1–2 nA amplitude, 3–5 ms duration, 0.7-1 Hz frequency, +/– a small holding current (<1.5 pA pF^{-1}, to gain an initial resting V_m of $\sim$-80 mV); parameters were kept constant throughout protocol. In some myocytes, [Ca^{2+}]$_i$ was measured concurrently with APs by epifluorescence microscopy, with ratiometric quantification of [Ca^{2+}]$_i$ using Fura-2 pentapotassium salt, 0.1 mM (with K$_2$EGTA then lowered

to 0.01 mM) via the patch pipette. Fluorescence was measured at 340 and 380 nm every 15 ms using a Cairn Optoscan monochromator (Cairn Research, Faversham, UK). Minimum (R_{min}) and maximum (R_{max}) fluorescence ratios (340/380 nm) were measured; cytoplasmic $[Ca^{2+}]$ was calculated as $K_d \times [(R - R_{min})/(R_{max} - R)]$, with K_d of 1.2 μM (Kettlewell *et al.* 2013).

Dynamic clamp technique

The dynamic clamp technique (Fig. 1) was used, during AP recording in rabbit and human atrial myocytes, to simulate systematic changes in the voltage-dependent characteristics of steady-state activation and inactivation of I_{CaL}. Native I_{CaL} was first inhibited with nifedipine (3 μM), then replaced by a mathematically modelled, dynamic clamp current, $I_{CaL,D-C}$. This current was computed in real-time, based on the myocyte's continuously monitored V_m during the AP, and injected into the cell via the patch-pipette (by adding it

to the AxoClamp 2B stimulus current pathway) at precisely-timed 50 μs intervals (update rate: 20 kHz). Because the $I_{CaL,D-C}$ injection in turn modifies the V_m, there is a bidirectional dynamic interaction between the AP waveform and $I_{CaL,D-C}$ (Fig. 1). The I_{CaL} model implemented in the dynamic clamp is a simplified version of that developed by Nygren *et al.* (1998) and exhibits exponential voltage-dependent activation, as well as bi-exponential inactivation with a fast component governed by $[Ca^{2+}]_i$. Equations (1)–(10) (shown in Fig. 1 in general form, and also below containing values obtained from the experiments) define I_{CaL}, governed by a voltage-dependent activation factor (d_L) and exhibiting a bi-exponential decay (f_{L1}, f_{L2}), with semi-empirical, steady-state activation ($\bar{d}_L$), inactivation ($\bar{f}_L$) and time constant curves ($\tau_d, \tau_{fL1}, \tau_{fL2}$); all tuned to the voltage- and time-dependent parameters of the native I_{CaL} (Fig. 2). In the absence of information on $[Ca^{2+}]_i$ accessible to the dynamic clamp, the Ca^{2+}-dependency of I_{CaL} inactivation was simplified by fixing f_{Ca} (determining
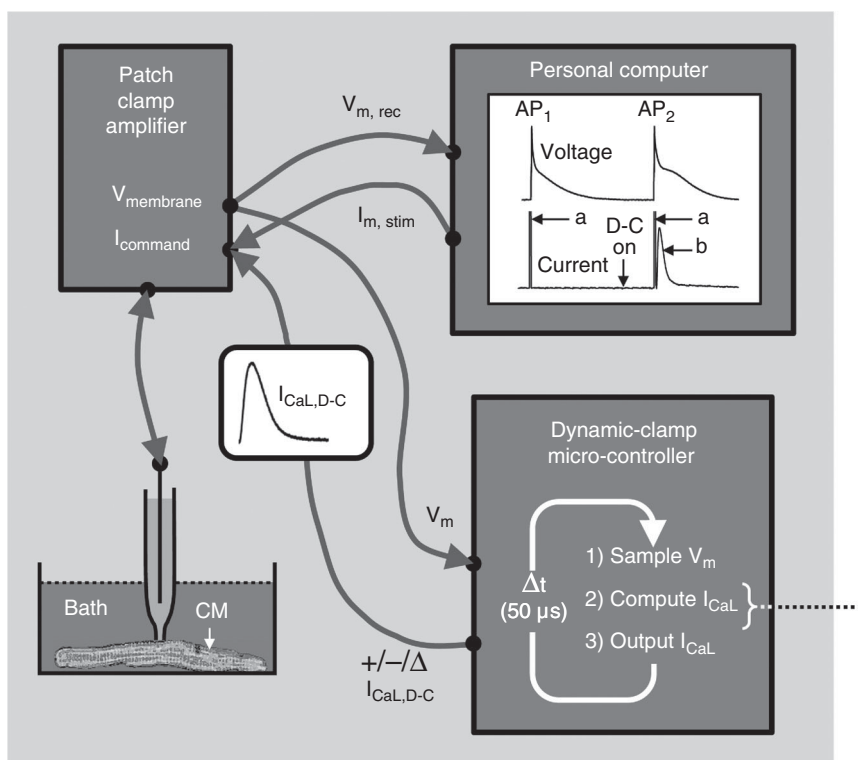
Figure 1. Dynamic clamp set-up and method
Personal computer (PC) running standard electrophysiology software to generate a train of short pulses ('a'), which are sent ($I_{m, stim}$) to input ($I_{command}$) of a patch clamp amplifier (PCA) instructing it to inject current pulses to elicit action potentials (AP) in an isolated cardiomyocyte (CM). The membrane voltage (V_m) change is measured by PCA and sent ($V_{m, rec}$) from PCA output ($V_{membrane}$) for display and recording on the PC (i.e. conventional AP recording) ('AP$_1$'). When the dynamic clamp (D-C) microcontroller is switched on ('D-C on'), it continuously samples V_m (from PCA $V_{membrane}$) during subsequent AP recording and, using Hodgkin–Huxley equations (eqns 1-10; definitions in the Methods), calculates a model L-type Ca^{2+} current (I_{CaL}) based on instantaneous V_m, which is updated and injected, as a dynamic clamp current ($I_{CaL,D-C}$), into the stimulus pathway (via $I_{command}$) at precisely timed 50 μs intervals. Because $I_{CaL,D-C}$ injection modifies V_m, and *vice versa*, there is a bidirectional dynamic interaction between the waveforms of the ensuing AP ('AP$_2$') and corresponding $I_{CaL,D-C}$ ('b'). Parameters in eqns (1)–(10) are initially set with control values measured in atrial cells (Fig. 2), then systematically changed to investigate effects of altering magnitude, polarity, voltage- and/or time-dependence of $I_{CaL,D-C}$ ('+/-/Δ $I_{CaL,D-C}$') on AP$_2$ and subsequent APs.

$$I_{Ca,L} = \bar{g}_{Ca,L} d_L [f_{Ca} f_{L1} + (1 - f_{Ca}) f_{L2}](V - E_{Ca}) \quad (1)$$

$$\bar{d}_L = \frac{1}{1 + e^{(V - V_{\bar{d}_L 0.5})/V_{\bar{d}_L slp}}} \quad (2)$$

$$\bar{f}_{L1} = \bar{f}_{L2} = \frac{1}{1 + e^{(V - V_{\bar{f}_L 0.5})/V_{\bar{f}_L slp}}} \quad (3)$$

$$\frac{dd_L}{dt} = \frac{\bar{d}_L - d_L}{\tau_{dL}} \quad (4) \qquad \frac{df_{L1}}{dt} = \frac{\bar{f}_{L1} - f_{L1}}{\tau_{L1}} \quad (5) \qquad \frac{df_{L2}}{dt} = \frac{\bar{f}_{L2} - f_{L2}}{\tau_{L2}} \quad (6)$$

$$f_{Ca} = \frac{[Ca^{2+}]_i}{[Ca^{2+}]_i + kCa} = 0.5 \quad (7) \qquad \tau_{dL} = (\tau_{dL,max} - \tau_{dL,min}) e^{-((V - V_{\tau_{dL,pk}})/V_{\tau_{dL,slp}})^2} + \tau_{dL,min} \quad (8)$$

$$\tau_{fL1} = (\tau_{fL1,max} - \tau_{fL1,min}) e^{-((V - V_{\tau_{fL1,pk}})/V_{\tau_{fL1,slp}})^2} + \tau_{fL1,min} \quad (9)$$

$$\tau_{fL2} = (\tau_{fL2,max} - \tau_{fL2,min}) e^{-((V - V_{\tau_{fL2,pk}})/V_{\tau_{fL2,slp}})^2} + \tau_{fL2,min} \quad (10)$$

relative proportion of fast and slow decay) at 0.5. The dynamic clamp was custom-built using a National Instruments CRIO-9076 real time controller, equipped with a 400 MHz PowerPC CPU, Xilinx Spartan 6 FPGA (Field Programmable Gate Array) and 16 bit A/D and D/A converters (National Instruments, Newbury, UK). The I_{CaL} model, executing on the FPGA, was written in LabVIEW (National Instruments) and the device controlled from a host computer via an RS232 interface. The user interface, for defining and controlling $I_{CaL,D-C}$ characteristics, was custom written: WinWCP DCLAMP (John Dempster). By systematically and independently shifting half-voltages ($V_{0.5}$) of $I_{CaL,D-C}$ activation and inactivation, via this interface, the effects of changing the $I_{CaL,D-C}$ window region on AP characteristics including EADs could be investigated. All effects were checked for reversibility upon removal of such $I_{CaL,D-C}$ interventions.

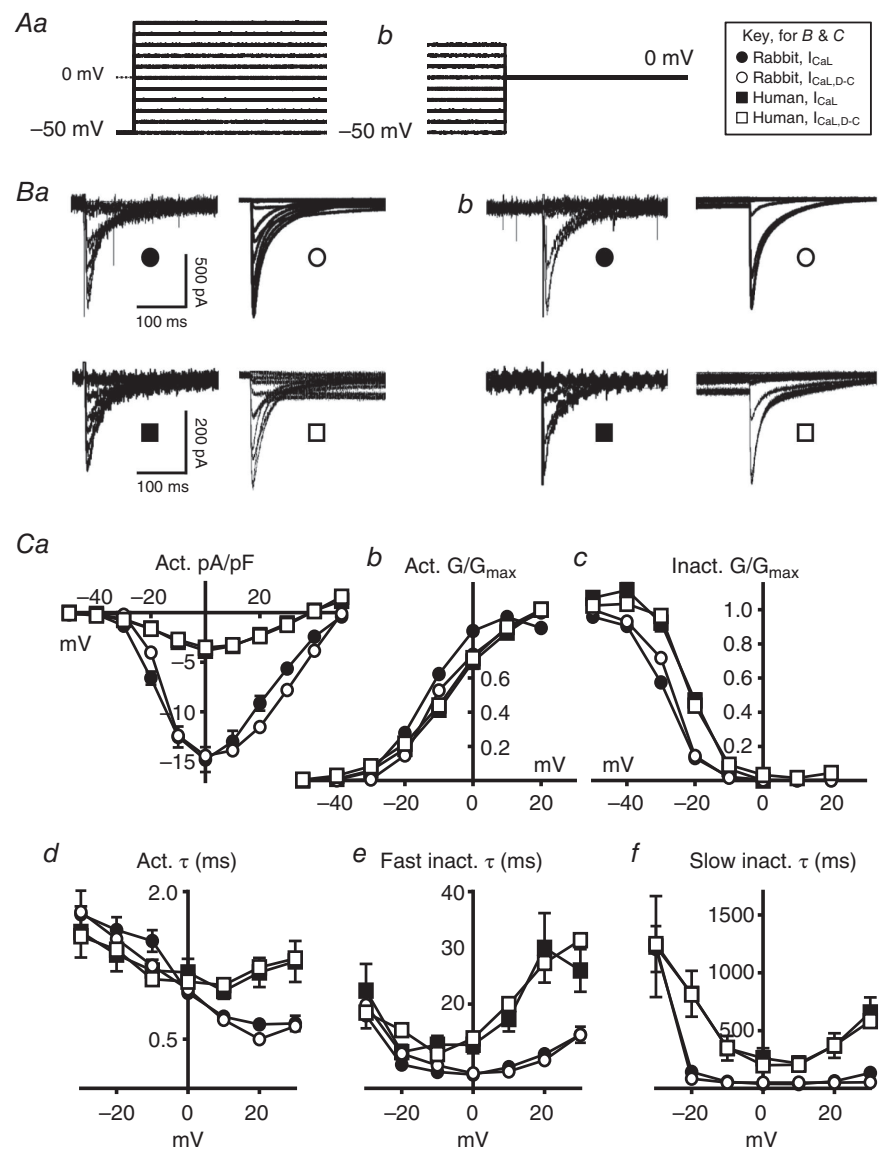## I_{CaL} models implemented in the dynamic clamp, containing values from the experimental data shown in Fig. 2

Rabbit:

$$I_{Ca,L} = \bar{g}_{Ca,L} d_L \left[f_{Ca} f_{L1} + (1 - f_{Ca}) f_{L2} \right] (V - 49.5) \quad (1)$$

$$\bar{d}_L = \frac{1}{1 + e^{(V+14.6)/4.5}} \quad (2)$$

$$\bar{f}_{L1} = \bar{f}_{L2} = \frac{1}{1 + e^{(V+28.3)/4.4}} \quad (3)$$

$$\frac{dd_L}{dt} = \frac{\bar{d}_L - d_L}{\tau_{dL}} \quad (4)$$

Figure 2. Comparison of live and simulated atrial I_{CaL} in rabbit and human

Circles, rabbit; squares, human. Filled symbols, live atrial cell data (I_{CaL}); open symbols, current generated by dynamic clamp I_{CaL} models ($I_{CaL,D-C}$). *A*, voltage protocols for steady-state activation (*Aa*) and inactivation (*Ab*) of I_{CaL} or $I_{CaL,D-C}$, producing currents in (*Ba*) and (*Bb*). *C*, mean ± SE voltage- and time-dependence of I_{CaL} activation and inactivation in live cells (*n* = 22–35 cells/four rabbits; 13–43 cells/seven patients), or $I_{CaL,D-C}$ from single simulation runs. *Ca*, steady-state activation current density. *Cb* and *Cc*, steady-state activation and inactivation conductance (G). *Cd*, activation time constant. *Ce* and *Cf*, fast and slow inactivation time constants.

$$\frac{df_{L1}}{dt} = \frac{\bar{f}_{L1} - f_{L1}}{\tau_{L1}} \tag{5}$$

$$\frac{df_{L2}}{dt} = \frac{\bar{f}_{L2} - f_{L2}}{\tau_{L2}} \tag{6}$$

$$f_{Ca} = \frac{[Ca^{2+}]_i}{[Ca^{2+}]_i + k_{Ca}} = 0.5 \tag{7}$$

$$\tau_{dL} = 0.0018 e^{-((V+21)/25)^2} + 0.0024 \tag{8}$$

$$\tau_{fL1} = 0.74 e^{-((V+29.6)/5.8)^2} + 0.066 \tag{9}$$

$$\tau_{fL2} = 29.49 e^{-((V-1)/1868)^2} + 29.5 \tag{10}$$

Human:

$$I_{Ca,L} = \bar{g}_{Ca,L} d_L \left[f_{Ca} f_{L1} + (1 - f_{Ca}) f_{L2} \right] (V - 38.4) \tag{1}$$

$$\bar{d}_L = \frac{1}{1 + e^{(V+6.5)/7.8}} \tag{2}$$

$$\bar{f}_{L1} = \bar{f}_{L2} = \frac{1}{1 + e^{(V+23)/3.8}} \tag{3}$$

$$\frac{dd_L}{dt} = \frac{\bar{d}_L - d_L}{\tau_{dL}} \tag{4}$$

$$\frac{df_{L1}}{dt} = \frac{\bar{f}_{L1} - f_{L1}}{\tau_{L1}} \tag{5}$$

$$\frac{df_{L2}}{dt} = \frac{\bar{f}_{L2} - f_{L2}}{\tau_{L2}} \tag{6}$$

$$f_{Ca} = \frac{[Ca^{2+}]_i}{[Ca^{2+}]_i + k_{Ca}} = 0.5 \tag{7}$$

$$\tau_{dL} = 0.008 e^{-((V+7.5)/52.3)^2} + 0.0023 \tag{8}$$

$$\tau_{fL1} = 6.01 e^{-((V-6.3)/88.3)^2} + 6.21 \tag{9}$$

$$\tau_{fL2} = 0.019 e^{-((V+9.2)/22.6)^2} + 0.023 \tag{10}$$

Strengths and weaknesses of the technique

A significant strength of the dynamic clamp technique is that, by simulating modification of a specific ion current in a real cell (rather than in a mathematical model), its effect on the AP waveform can be observed interacting with all the naturally occurring voltage- and time-dependent physiological processes, including those not yet discovered and incorporated into the models. This is not to say that dynamic clamping is without its own intrinsic limitations, with the main ones being: (i) Because the modelled ion channel current is injected through the patch pipette and is thus carried primarily by ions such as K^+, Cl^-, or aspartate, the 'chemical effects' of the specific ion current modelled (e.g. I_{CaL}), such as local increases in ion concentrations (e.g. Ca^{2+}) or signalling changes from conformational changes of the channel, are absent (Berecki *et al.* 2014). However, this can also be an opportunity to separate electrical effects from chemical effects of the current (Berecki *et al.* 2014), as in the present study. (ii) The model current (in this case, $I_{CaL,D-C}$) is based on voltage- and time-dependent parameters averaged from recordings made from multiple cells rather than from the individual cell being dynamic clamped. (iii) The dynamic clamp technique naturally shares some of the limitations of conventional voltage- and current clamp methods, such as the use of fixed intracellular and extracellular solutions, and artefacts of electrode resistance and capacitance (Prinz *et al.* 2004).

Statistical analysis

Electrophysiological and $[Ca^{2+}]_i$ data are expressed as the mean ± SE. Continuous data were compared, among three or more groups, using a Friedman repeated measures test, for non-parametric, matched data, followed by Dunn's multiple comparisons test. Unpaired data were compared using a Kruskal–Wallis test, followed by uncorrected Dunn's. Categorical data were compared using a chi-squared test with Yates' correction. $P < 0.05$ was considered statistically significant. All statistical and curve fitting analyses were performed using Prism, version 7.00 (GraphPad Software Inc., San Diego, CA, USA).

Results

Comparison of live and simulated atrial I_{CaL} in rabbit and human

L-type Ca^{2+} current (I_{CaL}) showed characteristic rapid, mono-exponential activation, and slow, bi-exponential decay, in rabbit and human atrial myocytes (Fig. 2*B* and *C*). Peak I_{CaL} density was 3.9-fold larger in rabbit than human (Fig. 2*Ca*), with corresponding G_{max} values of 15 nS (0.3 nS pF^{-1}) and 7 nS (0.1 nS pF^{-1}), respectively, but the voltage-dependence of steady-state activation was similar (Fig. 2*Cb*). Other voltage- and time-dependent I_{CaL} characteristics differed between species, mainly with human having a positively-shifted steady-state inactivation compared to rabbit (Fig. 2*Cc*), and also slower activation (Fig. 2*Cd*) and inactivation (Fig. 2*Ce* and *Cf*)

at positive potentials. Dynamic clamp currents ($I_{CaL,D-C}$), injected into a simple resistor (500 MΩ) capacitor (33 pF) circuit (Patch-1U model cell; Axon Instruments) and simulated in response to the same voltage pulse protocols (Fig. 2Aa and Ab), showed generally close agreement with the live cell data for all voltage- and time-dependent parameters (Fig. 2B and C).

Validation of the dynamic clamp technique for I_{CaL}

Native I_{CaL} was substantially inhibited, as shown in a rabbit atrial myocyte, using nifedipine (Fig. 3Aa). Nifedipine concentration—response curves (Fig. 3Ab) indicated complete inhibition of human atrial I_{CaL} (I_{max} 101%), but only partial inhibition in rabbit (I_{max}: 87%). Nifedipine at 3 μM, chosen as the highest concentration not substantially inhibiting currents other than I_{CaL} (e.g. I_{Kur} or I_{TO}) (Gao *et al.* 2005) was used in both species to allow dynamic clamp insertion of $I_{CaL,D-C}$ during AP recording. This inhibited native I_{CaL} by 91% in human and 68% in rabbit (Fig. 3Ab). In rabbit atrial cells, nifedipine removed a substantial portion of the AP plateau (Fig. 3Ba), with a corresponding marked decrease in APD_{50-90} (Fig. 3Bb), and also markedly decreased Ca^{2+} transient amplitude, CaT (Fig. 3Ca and Cb). Subsequent insertion of $I_{CaL,D-C}$, still with nifedipine superfusion, fully restored the plateau and all but the latest phases of repolarization (~APD_{90}) (Fig. 3Bb), and without further effect on CaT (Fig. 3Ca and Cb). Without nifedipine, subtraction of $I_{CaL,D-C}$, which offset the electrical (but not $[Ca^{2+}]_i$) effects of I_{CaL}, did not alter $[Ca^{2+}]_i$ (Fig. 3Ca and Cb) and produced similar APD_{50-70} changes as nifedipine, although it left a clear residual 'AP foot' (prolonged APD_{80-90} in Fig. 3Ba and Bb).

Mathematical modelling of the contribution to AP of electrical *vs.* Ca^{2+} changes from I_{CaL}

The relative contributions of purely electrical ($I_{CaL,D-C}$) *vs.* 'chemical' (Ca^{2+}) effects of I_{CaL}-reduction, as well as the likely cause of the 'AP foot' in the above ($I_{CaL,D-C}$ subtraction without nifedipine) experiment, were investigated using three published mathematical models of human atrial APs: 'CRN' (Courtemanche *et al.* 1998), 'Grandi' (Grandi *et al.* 2011) and 'Nygren'(Nygren *et al.* 1998) (Fig. 4). In each model, abolition of I_{CaL} (and thus Ca^{2+}-induced Ca^{2+}-release, CICR) abolished both the AP plateau (panels Aa, Ba and Ca) and inward $I_{Na/Ca}$ (panels Ab, Bb and Cb). However, compared to $I_{CaL,D-C}$-abolition in the presence of full $[Ca^{2+}]_i$-buffering (also abolishing CICR and inward $I_{Na/Ca}$), $I_{CaL,D-C}$-abolition alone only suppressed the plateau, with the difference (i.e. between dotted and dashed line pairs) being a result of inward $I_{Na/Ca}$. Qualitatively similar effects of 70% I_{CaL}- or

$I_{CaL,D-C}$-reduction on APs (panels Ac, Bc and Cc) and $I_{Na/Ca}$ (panels Ad, Bd and Cd) were observed, although generally attenuated compared to the 100% reductions, with 'Grandi' best qualitatively simulating (Fig. 4Bc) the 'AP foot' seen in rabbit atrial cells, accompanied by a relatively large inward $I_{Na/Ca}$.

### Effects of dynamic clamp-widening of the I_{CaL} window region on atrial AP waveforms

The overlapping region of the respective activation and inactivation curves 'N' in Fig. 5A (taken from Fig. 2Cb and Cc) signifies the normal $I_{CaL,D-C}$ window region. This is the V_m range within which a fraction of the current not inactivated may be available for reactivation. During continuous AP recording, insertion of normal-window $I_{CaL,D-C}$ resulted in a normal AP waveform ('N') in each of six rabbit and six human atrial myocytes (Fig. 5Ba and Bb, upper), with the corresponding $I_{CaL,D-C}$ 'N' shown beneath. Note that $I_{CaL,D-C}$ has opposite polarity to conventionally recorded I_{CaL} because it is injected into the cell. However, when the window region was progressively widened, in small (1 mV) steps, by simultaneously and equally (i.e. symmetrically) shifting half-voltages ($V_{0.5}$) of activation and inactivation (Fig. 5A), a variety of changes in AP waveforms was observed. In all 12 myocytes, initial window widening increased APD, accompanied by slowing of $I_{CaL,D-C}$ decay. As the window width was increased further, EADs were produced, either singly or with one or more subsequent oscillations, accompanied by $I_{CaL,D-C}$ reactivation (Fig. 5B). The take-off V_m of each single (or 1st-of-a-train) EAD ranged −22 mV to −16 mV in rabbit and −44 mV to −21 mV in human. The maximum V_m of this EAD or any subsequent oscillation(s) was −5 mV in rabbit and −8 mV in human; minimum V_m of any subsequent oscillation(s): −22 mV in rabbit, −28 mV in human. The maximum rate of rise of each EAD upstroke coincided with the peak of the corresponding reactivating current ($I_{CaL,D-C}$) and conductance ($G_{CaL,D-C}$) (Fig. 5C). In one of the rabbit atrial myocytes (Fig. 5Ba), initial window widening produced exclusively EADs that were followed by full repolarization (i.e. conventional EADs) then, with further widening, exclusively EADs on APs failing to repolarize (within BCL). In two of the rabbit myocytes, both EAD types were observed at same window widths, as it was progressively widened, and, in the other three, only EADs preceding non-repolarization occurred. Of the six human atrial myocytes, two showed a progressive shift from predominantly conventional EADs to predominantly EADs with non-repolarization (Fig. 5Bb), with four showing exclusively EADs with non-repolarization. All effects of window widening were reversed upon returning to normal-window width $I_{CaL,D-C}$ at the end of each protocol. Simulation of stepwise
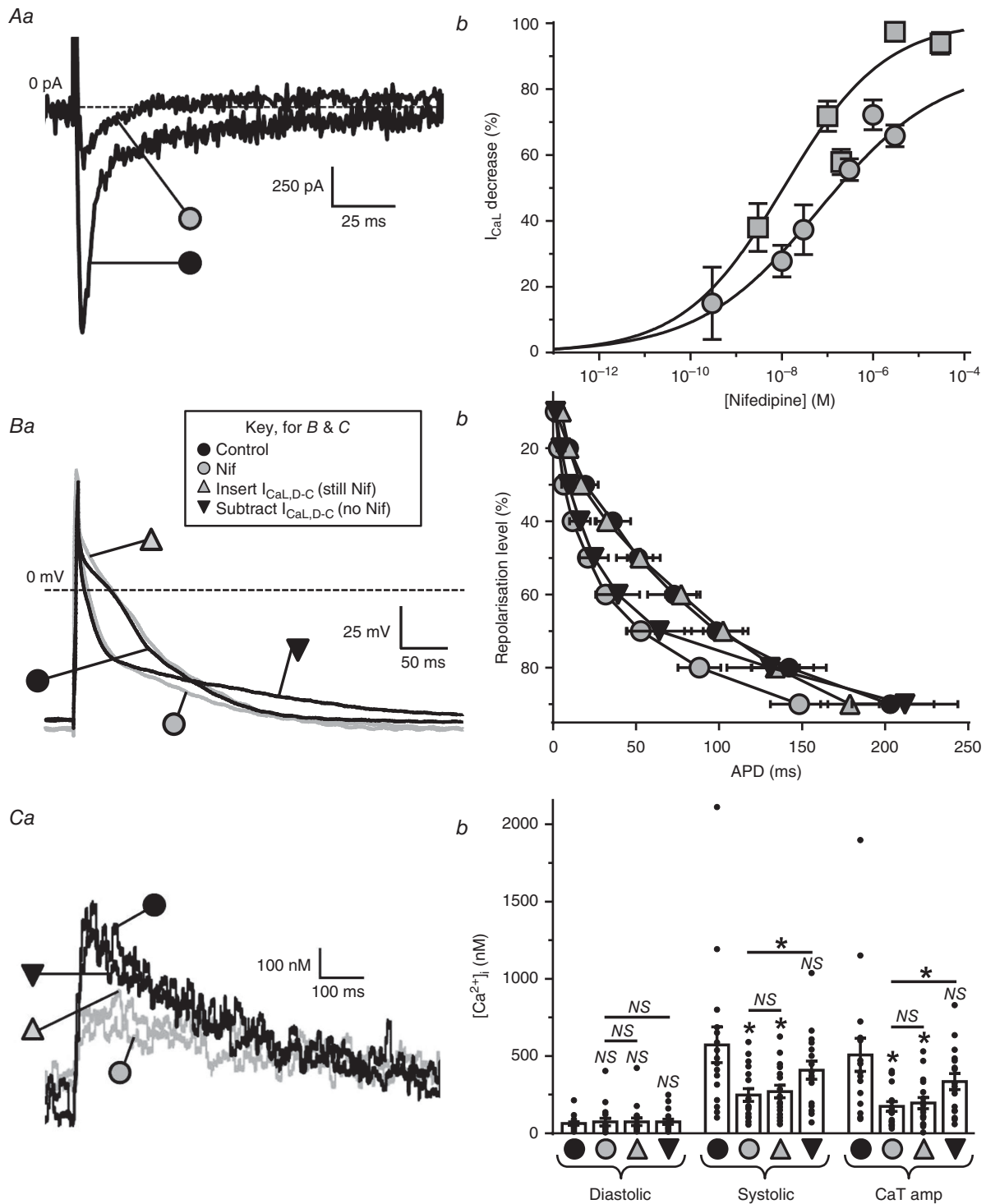
Figure 3. Validation of dynamic clamp technique for I_{CaL} in rabbit atrial cells
Grey symbols = nifedipine (Nif) present; black = Nif absent. *Aa*, original current traces showing typical maximal I_{CaL}-decrease by Nif (3 μM) in a rabbit atrial cell. *Ab*, Nif-I_{CaL} concentration–response curve for rabbit cells (n = 5–14, 3 or 4 rabbits; circles); with human cells (n = 10–22 cells/3 patients; squares) for comparison. *Ba*, representative superimposed APs from a single atrial cell before (●) and after (○) 3 μM Nif, during insertion of $I_{CaL,D-C}$ (G_{max} 15 nS) in the continued presence of Nif (△), and during subtraction of $I_{CaL,D-C}$ (G_{max} −15 nS) in the absence of Nif (▼). *Bb*, average AP duration (APD) in 19–22 cells/8 or 9 rabbits under the same conditions as (*Ba*). *Ca*, [Ca^{2+}]$_i$ transients (CaT) measured during AP recording under the same conditions as (*B*). *Cb*, average [Ca^{2+}]$_i$ in 17 cells/6 rabbits from (*Bb*). *P < 0.05 *vs.* controls, or between groups under lines; NS, not significant; Friedman & Dunn's multiple comparisons tests.
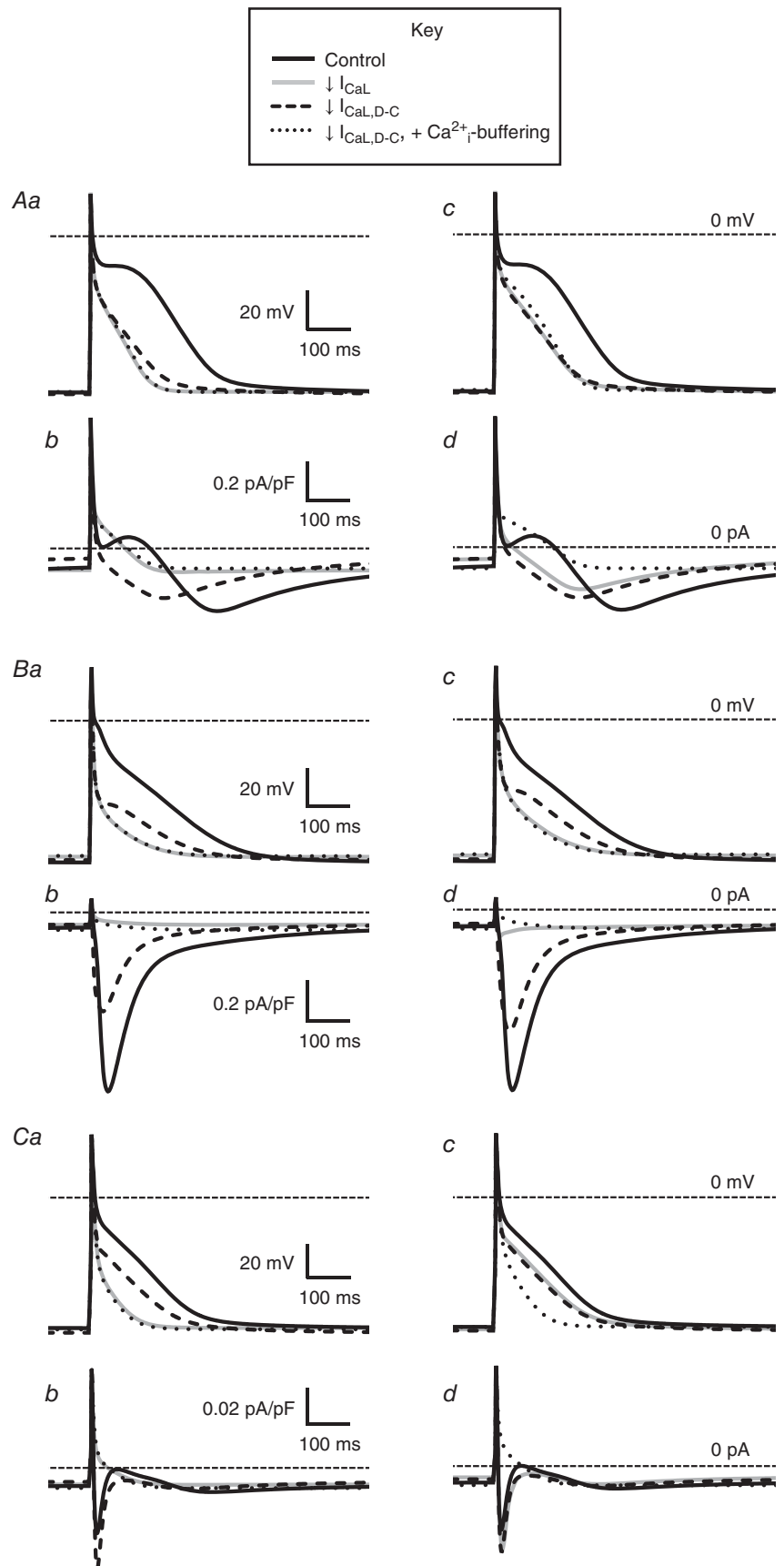
Figure 4. Mathematical modelling of the contribution to the AP waveform of electrical and Ca²⁺ changes from I_{CaL} decrease, and the involvement of $I_{Na/Ca}$

Action potentials (AP) and Na⁺/Ca²⁺-exchange currents ($I_{Na/Ca}$) simulated using mathematical models CRN (Courtemanche *et al.* 1998) (*A*), Grandi (Grandi *et al.* 2011) (*B*) and Nygren (Nygren *et al.* 1998) (*C*). *Aa*, *Ab*, *Ba*, *Bb*, *Ca* and *Cb*, superimposed APs and $I_{Na/Ca}$, respectively (1 Hz stimulation), under a 100% reduction in I_{CaL} or dynamic clamp I_{CaL} ($I_{CaL,D-C}$). *Ac*, *Ad*, *Bc*, *Bd*, *Cc* and *Cd* are APs and $I_{Na/Ca}$ under a 70% reduction in I_{CaL} or $I_{CaL,D-C}$. Solid black lines indicate the control; solid grey lines indicate I_{CaL} reduction (e.g. as from nifedipine); dashed black lines indicate $I_{CaL,D-C}$ reduction (i.e. isolated electrical component of I_{CaL} reduction); dotted black lines indicate $I_{CaL,D-C}$ reduction of 100% (*Aa*, *Ab*, *Ba*, *Bb*, *Ca* and *Cb*) or 70% (*Ac*, *Ad*, *Bc*, *Bd*, *Cc* and *Cd*) when holding [Ca²⁺]ᵢ at its diastolic level (100% Ca²⁺ buffering).
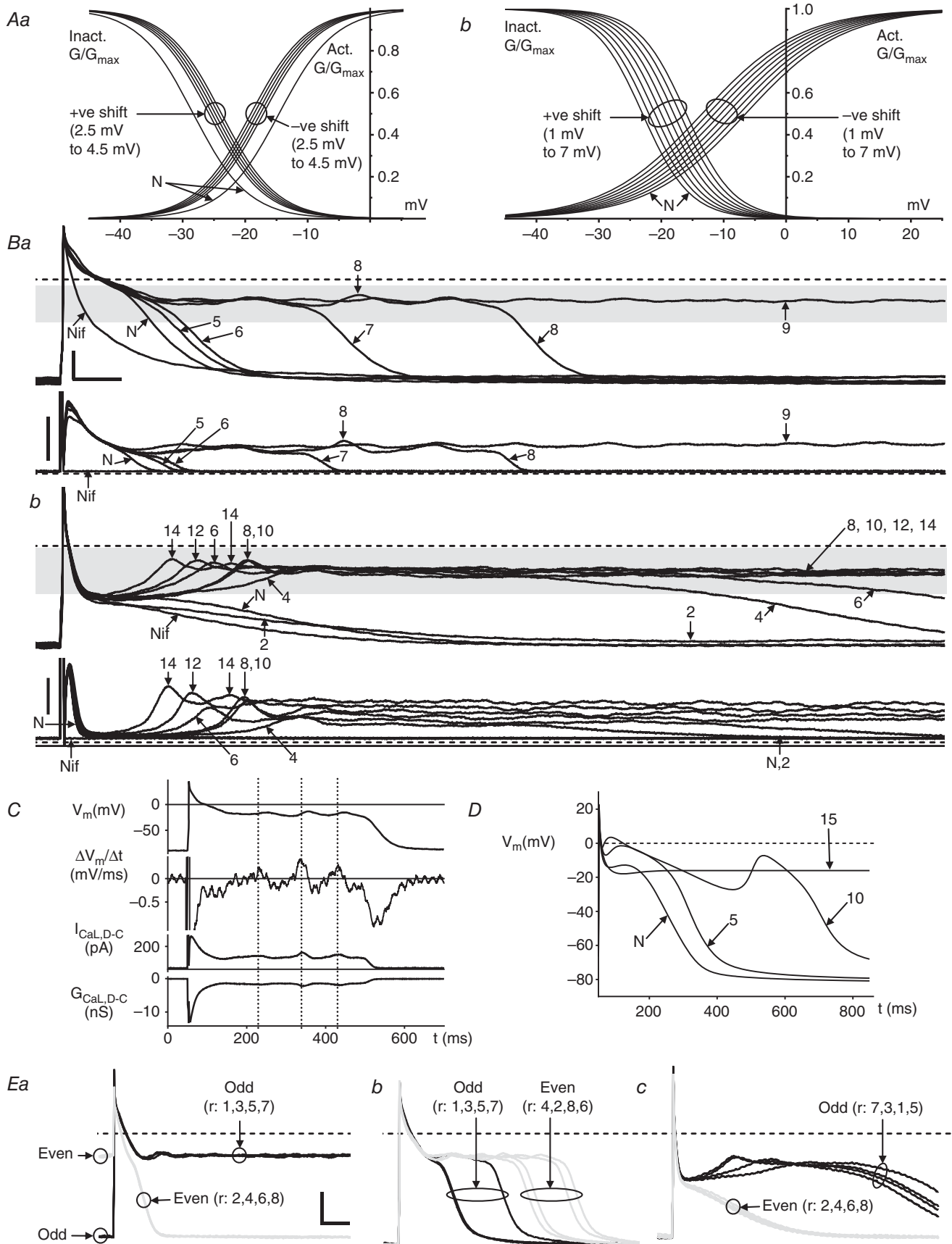
widening of the I_{CaL} window, using 'CRN' (Courtemanche *et al.* 1998), also produced progressive APD-increase, conventional EADs and, finally, repolarization failure (Fig. 5*D*). A further observation in the live cells, albeit uncommon, was a consistently repeating bi-alternation of AP-waveform: alternans (Fig. 5*E*). This occurred in three of 22 rabbit and two of 31 human atrial cells (includes cells from Fig. 6*E* and *F*), and featured both maximum diastolic potential (MDP)-alternans (Fig. 5*Ea*) and true APD-alternans (i.e. with no accompanying MDP-alternans) (Fig. 5*Eb* and *Ec*).

$I_{CaL,D-C}$ window width-dependence of EAD incidence in rabbit and human atrium

A systematic study of the effect of symmetrical widening of the $I_{CaL,D-C}$ window (Fig. 6*A*) on the incidence of the two different EAD types (as defined in Fig. 6*Ba* and *Bb*) showed a window width-dependence of EAD production in rabbit and human atrial myocytes. Note that the AP response-type in Fig. 6*Bc* displayed no EAD and so was not included in the analyses. Representative traces in Fig. 6*C* (rabbit) and *D* (human) illustrate the respective average data (Fig. 6*E* and *F*), showing that, after insertion of normal-window width $I_{CaL,D-C}$ to recover the AP plateau pre-supressed by nifedipine (Fig. 6*Ea* and *Fa*), increasing the window width (in 5 mV steps up to 15 mV in rabbit, 30 mV in human) produced a significant, stepwise, increase in the incidence of combined-type EADs (Fig. 6*Ec*: rabbit; Fig. 6*Fc*: human), with no significant effect on the incidence of solely conventional EADs (Fig. 6*Eb* and *Fb*).

Asymmetrical widening of the $I_{CaL,D-C}$ window produced EADs, particularly when shifting activation voltage

Widening $I_{CaL,D-C}$ window asymmetrically, by shifting independently (solely) either the activation or inactivation curves (e.g Fig. 7*A* for rabbit; Fig. 7*B* for human), also produced EADs, although preferentially from shifting activation. In rabbit, significant production of conventional EADs resulted from a 10 mV shift of either curve (Fig. 7*Ca* and *Eb*). Considering combined-type EADs (Fig. 7*Ca* and *Cb*), a significantly higher incidence resulted from negatively-shifting the activation curve compared to positively-shifting inactivation (Fig. 7*Ec*). Such a differential effect of activation *vs.* inactivation curve-shifting was also significant in human (Fig. 7*Da*, *Db* and *Fc*), and more pronounced than in rabbit, with no EADs resulting from a 15 mV shift in inactivation, yet with a 53% EAD incidence in response to an activation voltage-shift of same magnitude (Fig. 7*Fc*).

Narrowing the $I_{CaL,D-C}$ window abolished EADs evoked by increasing current conductance with or without 4-AP

In rabbit atrial myocytes ($n = 18$), increasing (by three-fold) the maximum conductance (G_{max}) of normal-window width $I_{CaL,D-C}$, which left the window region configuration entirely unaffected (Fig. 8*Aa*), produced EADs in six myocytes, with conventional-type in four, including multiple EADs (Fig. 8*Ba*). The time scale-expanded traces of Fig. 8*D* shows these V_m oscillations and associated $I_{CaL,D-C}$ reactivations, along with the same temporal relationship between peak $I_{CaL,D-C}$ and EAD upstroke as observed in the earlier (Fig. 5*C*) window widening experiments. In every cell, narrowing of the $I_{CaL,D-C}$ window (still at three-fold G_{max}) by 10 mV, by simultaneously and equally shifting $V_{0.5}$ activation (positively) and inactivation (negatively) (Fig. 8*Ab*), abolished all EADs of any type (Fig. 8*B* and *E*). This effect was at least partially reversible (e.g. Fig. 8*B*). In 10 of the 12 cells in which increasing $I_{CaL,D-C}$ alone did not produce EADs, 4-AP was subsequently superfused, which, in turn, produced EADs (Fig. 8*C*) in five cells. In each of those, the same window narrowing intervention, in the continued presence of increased $I_{CaL,D-C}$+4-AP, also abolished all EADs of any type (Fig. 8*C* and *F*). Combining the data ($n = 11$ myocytes) from either intervention affirmed the

---

Figure 5. Effects of dynamic clamp-widening of the I_{CaL} window on APs in rabbit and human
A, $I_{CaL,D-C}$-voltage curves used to progressively widen window region during recording of APs (*B*) by simultaneous stepwise shifting of half-voltages ($V_{0.5}$) of activation (negatively) and inactivation (positively) from normal (N), in rabbit (*Aa*) (widening by 5–9 mV in 1 mV steps, by 0.5 mV shifting of activation and inactivation) and human (*Ab*) (2–14 mV in 2 mV steps). *B*, superimposed APs (upper) and $I_{CaL,D-C}$ (lower) from a single rabbit (*Ba*) and human (*Bb*) atrial cell, recorded first with 3 μM nifedipine (Nif), then after inserting $I_{CaL,D-C}$ (N), followed by window widening by arrowed values (mV). AP responses to widening include EADs, and instances of non-repolarization; $I_{CaL,D-C}$ responses: associated reactivations, and non-inactivations. All traces at same scale (bars = 50 ms, 25 mV). Grey bands = window voltage ranges, as determined from (*Aa*) and (*Ab*), producing EADs. $I_{CaL,D-C}$ bar = 0.2 nA for (*Ba*), 0.1 nA for (*Bb*). *C*, temporal relationship of changes in V_m (top trace; from *Ba*, 8 mV widening), its first derivative ($\Delta V_m/\Delta t$), and D-C current ($I_{CaL,D-C}$) and conductance ($G_{CaL,D-C}$). *D*, mathematical simulation, using CRN (Courtemanche *et al.* 1998), of AP responses to widening I_{CaL} window by 5, 10 and 15 mV beyond N, showing production of APD-increase, EAD and non-repolarizing AP. *E*, sets of eight superimposed consecutive AP recordings (*r*: 1–8; black trace = odd *r* number, grey = even) from rabbit (*Ea* and *Eb*) and human (*Ec*), showing bi-alternation of MDP (*Ea*) or APD (*Eb* and *Ec*) after 10 mV window widening. Bars = 100 ms, 25 mV.
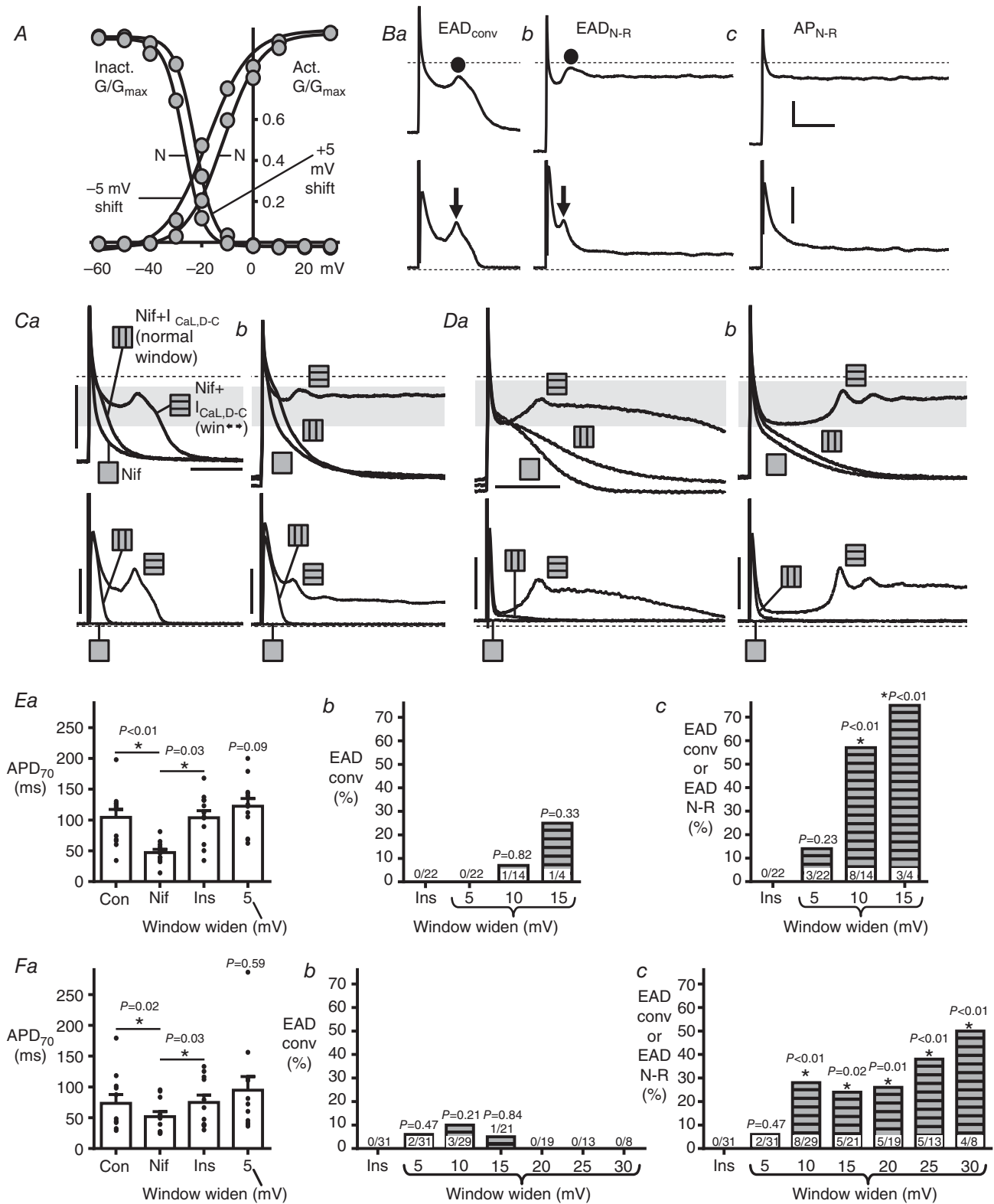
Figure 6. Symmetrical widening of the $I_{CaL,D-C}$ window produces EADs in rabbit and human atrial cells
A, $I_{CaL,D-C}$-voltage curves to widen window region during AP recording; in this case by 10 mV, in rabbit atrial, by simultaneously shifting activation $V_{0.5}$ –ve by 5 mV (vs. normal, N) and inactivation $V_{0.5}$ +ve 5 mV. B, EAD categorization for (C) to (F). Ba, EAD_{conv} = conventional EAD: clear transient depolarization in AP phase 2–3 followed by normal repolarization; Bb, EAD_{N-R} = EAD followed by non-repolarizing (within BCL) AP; Bc, AP_{N-R} = non-repolarizing AP without EAD. ● = EAD. ↓ = $I_{CaL,DC}$ reactivation. All traces (rabbit, 10 mV widening)

marked anti-EAD effect of narrowing the $I_{CaL,D-C}$ window region (Fig. 8*G*).

Discussion

We validated the dynamic clamp technique for investigating, for the first time to our knowledge, the electrical contribution of I_{CaL} to atrial APs, and then made the following key findings: widening the 'window' I_{CaL} region, particularly asymmetrically by shifting voltage-dependent I_{CaL} activation, produced EADs in a window width-dependent manner in rabbit and human atrial myocytes, with some instances of AP-alternans; and narrowing the I_{CaL} window abolished EADs that were produced by increasing I_{CaL} conductance and APD.

By informing and tuning the mathematical models of I_{CaL} used for dynamically injecting $I_{CaL,D-C}$, with the steady-state voltage- and time-dependent parameters of native I_{CaL} measured in the same cell types and under the same conditions as for dynamic clamping APs, this ensured an accurate and realistic representation of the native I_{CaL} during dynamic clamping APs. Some studies have used action potential clamping as a refinement of this step (e.g. for ventricular I_{Kr}) (Altomare *et al.* 2015). Because native I_{CaL} must be pharmacologically inhibited in order to replace it with $I_{CaL,D-C}$ for systematic study of manipulating the $I_{CaL,D-C}$ window and, because dynamic clamp cannot inject Ca^{2+}, there is no Ca^{2+}-induced Ca^{2+} release (CICR) during each AP. Therefore, a generalized (fixed) influence of Ca^{2+}-dependent inactivation of I_{CaL} (CDI) was included in $I_{CaL,D-C}$, by recording native I_{CaL} with minimal $[Ca^{2+}]_i$-buffering (low [EGTA] to buffer reagent-contaminating Ca^{2+} to ~physiological diastolic $[Ca^{2+}]_i$) (Fig. 3*C*) to permit the CaT during the initial voltage clamp experiments to affect the I_{CaL} waveform used to inform the model. $I_{CaL,D-C}$ did not, therefore, include a dynamically changing CDI. Other approaches to addressing CDI and absence of CICR when dynamic clamping have been to model subcellular $[Ca^{2+}]$ changes and feed back the influence of modelled CDI on the injected $I_{CaL,D-C}$ (Madhvani *et al.* 2011; Madhvani *et al.* 2015). Another consequence of CICR on the AP, $I_{Na/Ca}$, has not been injected along with $I_{CaL,D-C}$ in any study to date. We inhibited native I_{CaL} using the best available CCB

at the highest concentration possible without inhibiting important atrial repolarizing currents such as I_{Kur} and I_{TO} (i.e. nifedipine at 3 µM) (Gotoh *et al.* 1991; Gao *et al.* 2004; Gao *et al.* 2005). Whilst this substantially reduced I_{CaL} and CaT, it left a residual ~30% I_{CaL} in rabbit atrial cells and ~10% in human, which could be expected to produce a resulting component $I_{Na/Ca}$. Nevertheless, following nifedipine application in rabbit atrial myocytes, which substantially suppressed AP plateau and shortened APD, we found that $I_{CaL,D-C}$-insertion completely restored AP plateau and all but the latest phases of repolarization, thus validating $I_{CaL,D-C}$ for studying AP plateau and EADs. A recent simulation of 'chemical' *vs.* 'electrical' effects of $I_{Na/Ca}$-change on guinea-pig ventricular APs also suggests only a small contribution from $I_{Na/Ca}$ to late repolarization (Devenyi *et al.* 2017), although atrial APs were not studied. Conversely, in the present experiments, subtracting $I_{CaL,D-C}$ in the absence of nifedipine produced a residual 'AP-foot', suggestive of inward $I_{Na/Ca}$ under such a condition. Our mathematical modelling (with three AP models) (Courtemanche *et al.* 1998; Nygren *et al.* 1998; Grandi *et al.* 2011) of simultaneous APs and $I_{Na/Ca}$, with and without full $[Ca^{2+}]_i$-buffering, supported $[Ca^{2+}]_i$-induced $I_{Na/Ca}$ as the cause of this AP-foot under $I_{CaL,D-C}$ subtraction. Dynamic clamp-subtraction of ion currents has been used previously to attempt to overcome non-specificity of a pharmacological blocker (Workman *et al.* 2012) or to convert between AP waveform types (e.g. changing a mouse ventricular AP to a more human-like one using a calculated compensatory current) (Ahrens-Nicklas & Christini, 2009). Whilst dynamic clamp-subtraction of a suitable compensatory current (taking into account I_{CaL} and perhaps also $I_{Na/Ca}$) could be conceived as an alternative to using nifedipine (before superimposing additional I_{CaL} conductances with altered window characteristics), implementation and interpretation would be highly challenging and it was not attempted in the present study.

A variety of AP, EAD, alternans, and $I_{CaL,D-C}$ responses resulted from widening $I_{CaL,D-C}$ window; each consistent with a major contribution from window $I_{CaL,D-C}$ reactivation. The EADs were always accompanied by $I_{CaL,D-C}$-reactivation, and the coincidence of the $I_{CaL,D-C}$ and $G_{CaL,D-C}$ peak with the EAD upstroke maximum rate of rise is consistent with $I_{CaL,D-C}$ driving the EAD. The

at same scale: bar on AP = 25 mV; $I_{CaL,D-C}$ = 0.2 nA; time = 100 ms. APs (upper) and $I_{CaL,D-C}$ (lower) from (*C*) rabbit and (*D*) human, with 3 µM Nif (▢), insertion of $I_{CaL,D-C}$ with normal-window (▥), 10 mV widening (▤), showing production of EAD$_{conv}$ (*Ca* and *Da*) and EAD$_{N-R}$ (*Cb* and *Db*). Bars = 50 mV for APs; 0.2 nA for rabbit $I_{CaL,D-C}$, 0.1 nA for human; 100 ms for rabbit; 200 ms for human. Grey bands = window voltage ranges, from $I_{CaL,D-C}$-voltage curves, producing EADs. Average AP and EAD from rabbit (*E*) and human (*F*). *Ea* and *Fa*, APD$_{70}$ (for APs without EADs) in control (Con), following Nif, then $I_{CaL,D-C}$-insertion (Ins) and 5 mV widening; n = 12 cells/6 rabbits, 11 cells/8 patients. Incidences of cells displaying EAD$_{conv}$ (*Eb* and *Fb*) or EAD$_{conv}$/EAD$_{N-R}$ (*Ec* and *Fc*) after $I_{CaL,D-C}$-insertion and progressive window widening (5–15 mV in rabbit; 5–30 mV human). Values within bars: cell n (3–6 rabbits/4–8 patients). *P*: compares groups under horizontal lines, or *vs.* 'Ins'. Friedmans, Dunn's multiple comparisons, chi-squared tests.
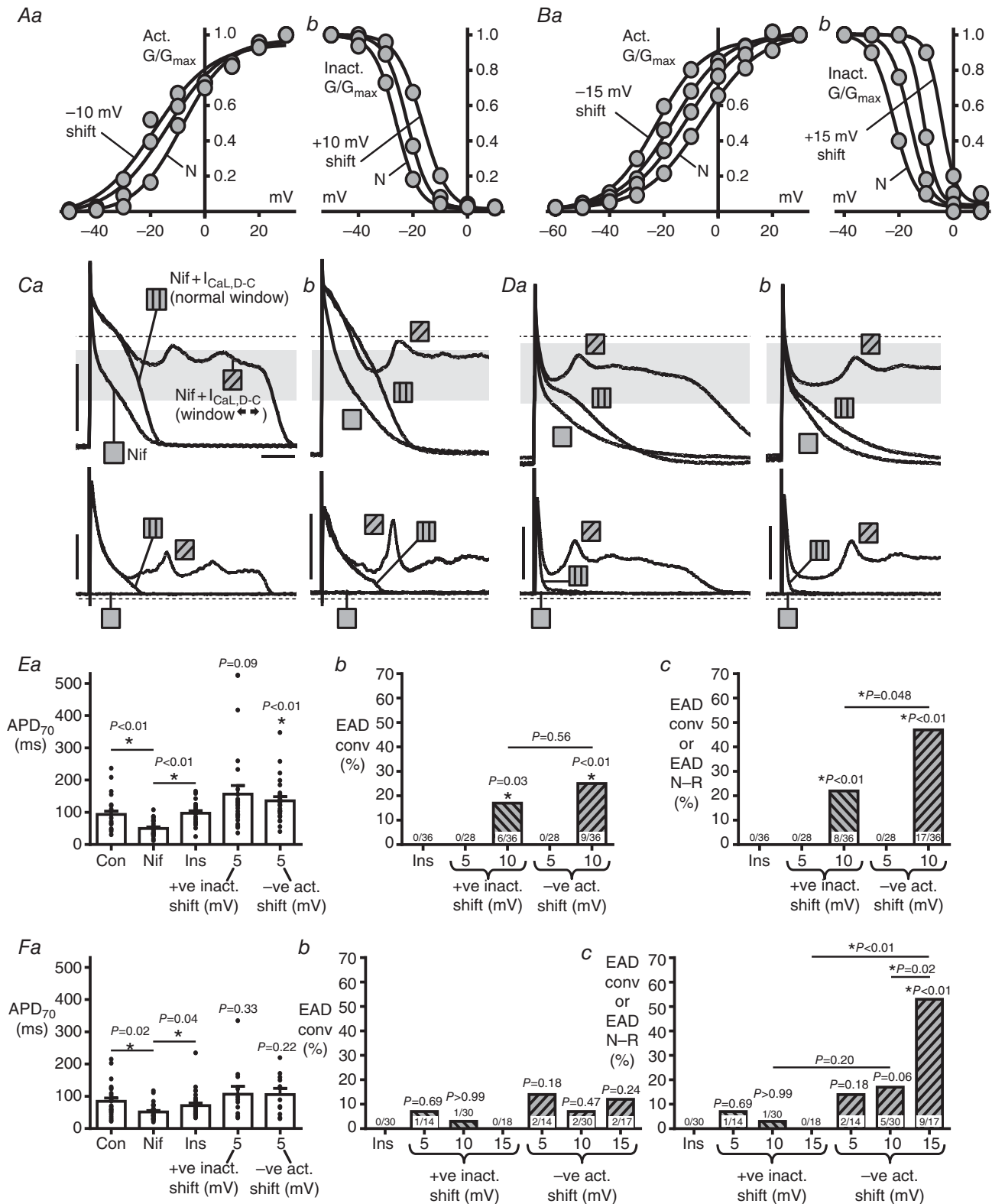
Figure 7. Asymmetrical widening of $I_{CaL,D-C}$ window, particularly by shifting activation voltage, produces EADs

$I_{CaL,D-C}$-voltage curves used for rabbit (*A*) and human (*B*), showing $V_{0.5}$ shifts of (*Aa* and *Ba*) activation and (*Ab* and *Bb*) inactivation (5 mV steps *vs.* N) to asymmetrically widen the $I_{CaL,D-C}$-window during AP recording. APs (upper) and $I_{CaL,D-C}$ (lower) from (*C*) rabbit and (*D*) human, with 3 μM Nif (▢), insertion of $I_{CaL,D-C}$ with normal-window (▥) then −10 mV activation shift (▧), showing EAD$_{conv}$ (*Ca* and *Da*) and EAD$_{N-R}$ (*Cb* and *Db*).

two main conditions for EAD production by window I_{CaL} reactivation (January & Riddle, 1989; Fozzard, 1992) were met, namely APD-increase (allowing $I_{CaL,D-C}$ to dwell in the window region long enough to reactivate) and the EADs oscillating within a voltage range allowing $I_{CaL,D-C}$-activation. For a contribution to these EADs from any inward $I_{Na/Ca}$ (from any residual CICR), EAD take-off potential would need to be negative to $E_{Na/Ca}$, which is expected to be positive to ~ -30 to -35 mV (Bers, 2002). Because the EADs in rabbit atrial myocytes (in which any residual CICR would be the larger) arose from potentials positive to $E_{Na/Ca}$, this suggests they were caused mainly or solely by window $I_{CaL,D-C}$ reactivation. Some of the human atrial EADs arose from potentials negative to $E_{Na/Ca}$, and so a potential contribution from inward $I_{Na/Ca}$ to their upstroke cannot be excluded. However, any such contribution may be expected to be relatively small because native I_{CaL} was >90% inhibited. Furthermore, because $I_{Na/Ca}$ decreases with depolarization, it cannot act regeneratively to enhance EAD amplitude unless $[Ca^{2+}]_i$ increases to maintain its driving force (Qu *et al.* 2013); unlike I_{CaL}, which increases with depolarization up to 0 or $+10$ mV and reactivates regeneratively. Whether or not there was a contribution from $I_{Na/Ca}$, it is clear that the electrical effect alone of widening the I_{CaL} window was sufficient, if not necessary, to generate EADs. These EADs were produced, in rabbit and human atrial myocytes, by symmetrical widening I_{CaL} window by simultaneously and equally shifting $V_{0.5}$ of activation (negatively) and inactivation (positively). However, we found a strong EAD-generating effect also resulted from shifting activation $V_{0.5}$ alone (i.e. with asymmetrical-widening). Because this effect was stronger than with shifting inactivation $V_{0.5}$ alone, it suggests that the ability of a reactivating I_{CaL} to generate EADs is more dependent on a larger I_{CaL} arising from more negative potentials (in line with holding potential-dependence of I_{CaL}) (Li & Nattel, 1997) than on a relatively small I_{CaL}-increase permissible from shifting the inactivation curve towards values around the peak for I_{CaL} (0 or $+10$ mV).

Each of the responses to window widening, whether a single EAD or multiple EAD oscillations followed by normal repolarization, a single EAD or multiple EADs followed by repolarization failure, or indeed repolarization failure with no EAD but rather a non-oscillating voltage signal (typically at V_m of the I_{CaL} window centre), can be considered in terms of a 'Hopf bifurcation' model of EADs (Qu *et al.* 2013). This model features analogous oscillations and 'basin of attraction' equilibrium states, including repolarization failure and 'bi-stable' states of MDP-alternans. The model emphasizes the major influence of I_{CaL} in non-linear dynamical processes necessary for EADs. It also highlights, however, the necessity of highly complex interactions between numerous ion currents and their gating variables for EADs to occur. This re-enforces the utility of dynamic clamping for studying EAD mechanisms because such complex interactions, and those not yet discovered, occur physiologically in the myocyte.

Cardiomyocytes require isolation for measuring ion currents or dynamic clamping APs, but this removes the syncytial current sink that occurs *in vivo*. This sink should be expected to overcome the repolarization failure observed to follow many of the cellular EADs here, and also perhaps to dampen the EADs themselves. However, the inward current producing these cellular events would still influence net source-to-sink ratio in the direction of APD-increase and EAD-generation. Whether that could contribute to arrhythmias in tissues is under debate. Weiss *et al.* (2010) propose that, although thousands of adjacent cells need synchronized EADs to produce a threshold propagating premature AP, this synchronization can occur naturally from the interaction between the divergent influence of chaos driving irregular EADs and the convergent influence of electrotonic coupling via gap junctions. Synchronization of chaotic EADs could also amplify APD-dispersion, forming 'EAD islands' next to regions without EADs, creating unidirectional conduction block and reentry. This self-organizing system could simultaneously create trigger and substrate for reentry even when the tissue is homogeneous, although they would develop more rapidly in heterogeneous tissue (e.g. fibrosed, aged atrium). Coupling between myocytes and myofibroblasts could also aid EAD production, demonstrated by dynamic clamping rabbit ventricular myocytes with an analogous virtual gap junction current (Nguyen *et al.* 2012).

To test whether $I_{CaL,D-C}$ window narrowing could suppress or prevent EADs, we induced EADs either by increasing the conductance of an injected $I_{CaL,D-C}$ having a normal window (as produced, for example, by adrenergic stimulation) (Workman, 2010) or, in myocytes then failing to generate EADs, adding the APD-prolonging

Bars (all traces) = 50 mV, 0.1 nA, 100 ms. Grey bands = window voltage ranges, as determined from (*A*) and (*B*), producing EADs. Average AP and EAD from rabbit (*E*) and human (*F*). *Ea* and *Fa*, APD_{70} in control (Con), following Nif, $I_{CaL,D-C}$-insertion (Ins) and a subsequent $+5$ mV shift in $V_{0.5}$ inactivation or, separately, a -5 mV activation shift ($n=26$ cells/9 rabbits, 11–28 cells/4–10 patients; Friedman or Kruskal–Wallis, Dunn's tests). Incidences of cells displaying EAD_{conv} (*Eb* and *Fb*) or EAD_{conv}/EAD_{N-R} (*Ec* and *Fc*) after $I_{CaL,D-C}$-insertion and subsequent act/inactivation $V_{0.5}$ shifting (5 mV steps). $n = 9$ or 10 rabbits/4–10 patients. *P*: compares groups under lines, or *vs.* Ins.
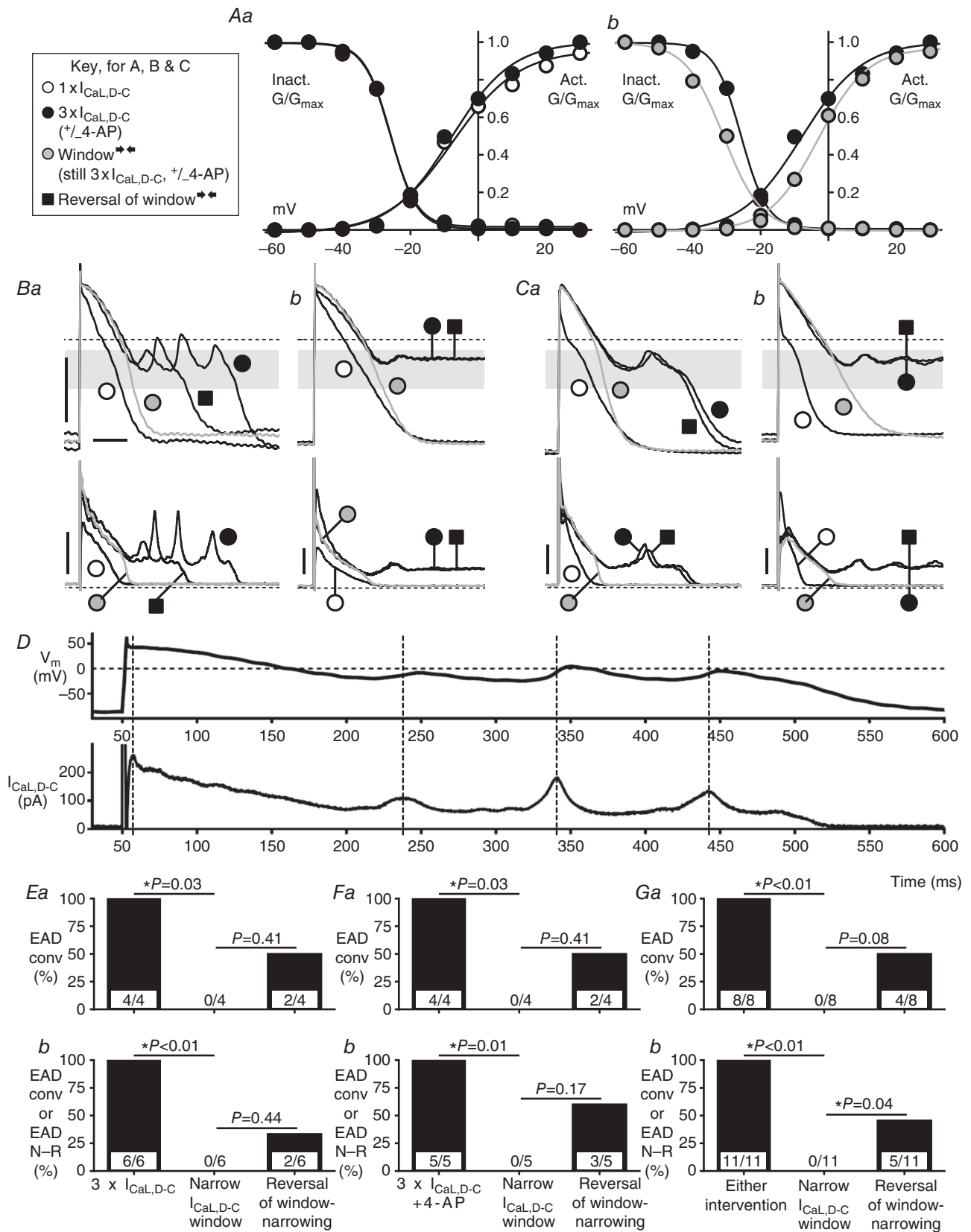
Figure 8. Narrowing $I_{CaL,D-C}$ window abolishes EADs from increased $I_{CaL,D-C}$ and/or 4-AP in rabbit

influence of K^+ current-block from 4-AP (Workman *et al.* 2000). These interventions should promote EADs by increasing reactivating current amplitude and dwell-time, respectively (January & Riddle, 1989; Fozzard, 1992; Devenyi *et al.* 2017). The $I_{CaL,D-C}$ window narrowing intervention then applied, comprising a simultaneous equal shift of $V_{0.5}$ of $I_{CaL,D-C}$ activation (positively) and inactivation (negatively), favoured shifting activation over inactivation in the window region itself, resulting in a rather asymmetrical window narrowing. This abolished all EADs, whether single, multiple, or preceding repolarization failure, presumably by affecting the portion of the window region (the left-activation-limb) shown above to be most sensitive for EAD production; preventing I_{CaL} reactivation. Although window I_{CaL} characteristics are determined partly by parameters additional to $V_{0.5}$ of activation and inactivation curves, previous studies (Madhvani *et al.* 2011; Madhvani *et al.* 2015) on EADs in rabbit ventricle support the view that it is the altering of these $V_{0.5}$ values, rather than the slopes of these curves or the kinetics of current activation or decay, which suppress EADs. EAD suppression from dynamic clamp reduction of a non-inactivating 'pedestal' I_{CaL} (increased by H_2O_2) was also shown (Madhvani *et al.* 2015), which is a component of I_{CaL} that we did not detect or model in atrial myocytes.

Pathological changes to window I_{CaL} have been reported, in the ventricle. In dogs, chronic atrioventricular block-induced hypertrophy was associated with window I_{CaL}-widening and EADs under β-adrenergic stimulation (Antoons *et al.* 2007). A genetic mutation in a patient with Timothy syndrome, a rare multigenetic disorder including QT-prolongation, may also cause window I_{CaL}-widening, APD-increase and EADs (Boczek *et al.* 2015). In atrium, although I_{CaL} is markedly altered in terms of peak current density (reduced) and open probability (increased) in human chronic AF (i.e. electrophysiological remodelling) (Klein *et al.* 2003; Workman *et al.* 2008; Heijman *et al.* 2014), there are no reports, to our knowledge, of pathological changes in window I_{CaL} voltage-dependence. Enhancement of atrial window I_{CaL} (e.g. from a pathological widening of the window region and/or an increase in I_{CaL} preferentially in the window

region) is unlikely to be a mechanism contributing to EAD production in clinical AF. However, it should be recognized that a therapeutically effective anti-AF target does not require to be one that is pathologically altered, as evidenced by the two most effective anti-AF drugs (amiodarone and flecainide), which are not considered to be effective by opposing the most prominent pathological ion current alterations (namely decreased I_{CaL} and I_{TO}, and increased I_{K1}) (Workman *et al.* 2011). Furthermore, a drug may be (and may be intended to be) more effective in un-remodelled atrium (as investigated in the present study); for example, in the treatment of new-onset or paroxysmal AF.

We propose that narrowing of a non-enhanced (and non-remodelled) I_{CaL} window may be considered as a potential therapeutic mechanism to inhibit atrial EADs caused by any primary mechanism, because of the likely prominent contribution ultimately (secondarily) of window I_{CaL} reactivation to such EADs. For example, I_{CaL} reactivation could occur with a sufficiently large increase in AP plateau duration, such as could result from adrenergic stimulation of I_{CaL} (Workman, 2010) (hence the present investigation of increasing $I_{CaL,D-C}$), K^+ current reduction or inhibition (Workman *et al.* 2001) (hence our use of 4-AP) or early (2–3 weeks) heart failure (Stambler *et al.* 2003; Yeh *et al.* 2008), all of which have potential relevance to AF. However, it must be recognized that dynamic clamping can assess only electrical (i.e. in the absence of CICR) effects of changing the current, and this is true for increasing $I_{CaL,D-C}$ conductance to provoke EADs, as well as for narrowing window I_{CaL} to prevent EADs. Alternatives to increasing $I_{CaL,D-C}$ could be considered in future studies, such as oxidative stress (Sato *et al.* 2009; Madhvani *et al.* 2011; Zhao *et al.* 2012; Madhvani *et al.* 2015) or hypo-kalaemia (Madhvani *et al.* 2011; Madhvani *et al.* 2015), as used previously in the ventricle.

The potential clinical therapeutic utility of window I_{CaL} narrowing is supported by recent reviews (Karagueuzian *et al.* 2017; Ortega *et al.* 2018) and based on the expectation (from modelling: Madhvani *et al.* 2011; Madhvani *et al.* 2015; Karagueuzian *et al.* 2017) that this intervention is unlikely to substantially affect $[Ca^{2+}]_i$

A, $I_{CaL,D-C}$-voltage curves to narrow window region during AP recording. *Aa*, activation/inactivation curves, of normal window width, from either $1 \times I_{CaL,D-C}$ G_{max}: 15 nS (O) or $3 \times G_{max}$: 45 nS (●); window unaltered by the G_{max}-increase. *Ab*, comparison of the normal-width 45 nS curves (●) *vs.* 45 nS curves with window narrowed by simultaneously shifting $V_{0.5act}$ +5 mV and $V_{0.5inact}$ -5 mV (O). *B* and *C*, APs (upper) and $I_{CaL,D-C}$ (lower), all with Nif to supress I_{CaL}. 15 nS $I_{CaL,D-C}$ with normal-window (O), then EAD_{conv} (*Ba* and *Ca*) or EAD_{N-R} (*Bb* and *Cb*) were evoked, either by trebling $I_{CaL,D-C}$ (*B*) or, in different cells, by trebling $I_{CaL,D-C}$ and adding 4-aminopyridine (4-AP; 2 mM) (*C*) (●). Then, the $I_{CaL,D-C}$ window was narrowed (O), still with G_{max} 45 nS (and 4-AP if applicable). Finally, window narrowing was reversed (■). Bars = 50 mV, 0.1 nA, 100 ms. Grey bands = window voltage ranges, as determined from (*Aa*), producing EADs. *D*, timescale expansion of traces ● from (*Ba*), showing $I_{CaL,D-C}$–V_m temporal relationship during EAD-formation. *E–G*, effect of window narrowing (and its reversal) on incidences of cells displaying EAD_{conv} (*Ea*, *Fa* and *Ga*), or EAD_{conv}/EAD_{N-R} (*Eb*, *Fb* and *Gb*), evoked by $3 \times I_{CaL,D-C}$ (*E*) or, in different cells, $3 \times I_{CaL,D-C}$ + 4-AP (*F*), or either intervention (*G*). $n = 2$ rabbits in (*E*), $n = 3$ rabbits in (*F*), $n = 5$ rabbits in (*G*).

and thus excitation-contraction coupling. By contrast, traditional CCBs (e.g. verapamil, dihydropyridines), although blocking window I_{CaL} to some extent, block peak and window I_{CaL} indiscriminately (i.e. with no preferential effect in the window voltage range). Inhibition of normally activating (not re-activating) I_{CaL} (i.e. peaking at voltages largely positive to the window region), depresses excitation–contraction coupling, and thus limits therapeutic value, particularly in patients with compromised cardiac function. Future studies of any candidate window I_{CaL} narrowing drug(s) should assess their effects on all aspects of atrial excitation–contraction coupling, and using a variety of EAD-promoting interventions. These could include, as studied in ventricle, $[Ca^{2+}]_i$-overload from isoprenaline and/or BayK 8644 (January & Riddle, 1989; Zhao *et al.* 2012), as well as oxidative stress, hypokalaemia or heart failure.

The present dynamic clamp study of I_{CaL}, the first to our knowledge in atrial cells, has identified a potentially anti-arrhythmic (in isolated cells, at least) ion current (electrical component) mechanism of action. If new drugs could be developed (or existing ones identified or modified) that preferentially target the I_{CaL} window region, by shifting voltage-dependent activation and/or inactivation curves with the result of narrowing the I_{CaL} window, without substantially affecting $[Ca^{2+}]_i$ and thus excitation–contraction coupling, and with minimal adverse effects, then these drugs could be much needed candidates for testing for anti-AF action, *in vitro* and *in vivo*.

References

Ahrens-Nicklas RC & Christini DJ (2009). Anthropomorphizing the mouse cardiac action potential via a novel dynamic clamp method. *Biophys J* **97**, 2684–2692.

Altomare C, Bartolucci C, Sala L, Bernardi J, Mostacciuolo G, Rocchetti M, Severi S, & Zaza A (2015). I_{Kr} impact on repolarization and its variability assessed by dynamic clamp. *Circ Arrhythm Electrophysiol* **8**, 1265–1275.

Antoons G, Volders PGA, Stankovicova T, Bito V, Stengl M, Vos MA, & Sipido KR (2007). Window Ca^{2+} current and its modulation by Ca^{2+} release in hypertrophied cardiac myocytes from dogs with chronic atrioventricular block. *J Physiol* **579**, 147–160.

Berecki G, Verkerk AO, van Ginneken ACG, & Wilders R (2014). Dynamic clamp as a tool to study the functional effects of individual membrane currents. *Methods Mol Biol* **1183**, 309–326.

Bers DM (2002). Cardiac excitation-contraction coupling. *Nature* **415**, 198–205.

Boczek NJ, Miller EM, Ye D, Nesterenko VV, Tester DJ, Antzelevitch C, Czosek RJ, Ackerman MJ, & Ware SM (2015). Novel Timothy syndrome mutation leading to increase in *CACNA1C* window current. *Heart Rhythm* **12**, 211–219.

Burashnikov A & Antzelevitch C (2003). Reinduction of atrial fibrillation immediately after termination of the arrhythmia is mediated by late phase 3 early afterdepolarization-induced triggered activity. *Circulation* **107**, 2355–2360.

Colman MA, Ni H, Liang B, Schmitt N, & Zhang H (2017). *In silico* assessment of genetic variation in *KCNA5* reveals multiple mechanisms of human atrial arrhythmogenesis. *PLoS Comput Biol* **13**, e1005587.

Courtemanche M, Ramirez RJ, & Nattel S (1998). Ionic mechanisms underlying human atrial action potential properties: insights from a mathematical model. *Am J Physiol Heart Circ Physiol* **275**, H301–H321.

Devenyi RA, Ortega FA, Groenendaal W, Krogh-Madsen T, Christini DJ, & Sobie EA (2017). Differential roles of two delayed rectifier potassium currents in regulation of ventricular action potential duration and arrhythmia susceptibility. *J Physiol* **595**, 2301–2317.

Fozzard HA (1992). Afterdepolarizations and triggered activity. In *Cardiac Adaptation in Heart Failure*, ed. Holtz J, Drexler H & Just H, pp. 105–113. Steinkopff Verlag, Darmstadt.

Gao Z, Lau CP, Chiu SW, & Li GR (2004). Inhibition of ultra-rapid delayed rectifier K^+ current by verapamil in human atrial myocytes. *J Mol Cell Cardiol* **36**, 257–263.

Gao Z, Sun H, Chiu SW, Lau CP, & Li GR (2005). Effects of diltiazem and nifedipine on transient outward and ultra-rapid delayed rectifier potassium currents in human atrial myocytes. *Br J Pharmacol* **144**, 595–604.

Gotoh Y, Imaizumi Y, Watanabe M, Shibata EF, Clark RB, & Giles WR (1991). Inhibition of transient outward K^+ current by DHP Ca^{2+} antagonists and agonists in rabbit cardiac myocytes. *Am J Physiol Heart Circ Physiol* **260**, H1737–H1742.

Grandi E, Pandit SV, Voigt N, Workman AJ, Dobrev D, Jalife J, & Bers DM (2011). Human atrial action potential and Ca^{2+} model: sinus rhythm and chronic atrial fibrillation. *Circ Res* **109**, 1055–1066.

Grundy D (2015). Principles and standards for reporting animal experiments in *The Journal of Physiology* and *Experimental Physiology*. *J Physiol* **593**, 2547–2549.

Guo D, Young L, Wu Y, Belardinelli L, Kowey PR, & Yan GX (2010). Increased late sodium current in left atrial myocytes of rabbits with left ventricular hypertrophy: its role in the genesis of atrial arrhythmias. *Am J Physiol Heart Circ Physiol* **298**, H1375–H1381.

Heijman J, Voigt N, Nattel S, & Dobrev D (2014). Cellular and molecular electrophysiology of atrial fibrillation initiation, maintenance, and progression. *Circ Res* **114**, 1483–1499.

January CT & Riddle JM (1989). Early afterdepolarizations: mechanism of induction and block. A role for L-type Ca^{2+} current. *Circ Res* **64**, 977–990.

Karagueuzian HS, Pezhouman A, Angelini M, & Olcese R (2017). Enhanced late Na and Ca currents as effective antiarrhythmic drug targets. *Front Pharmacol* **8**, 36.

Kettlewell S, Burton FL, Smith GL, & Workman AJ (2013). Chronic myocardial infarction promotes atrial action potential alternans, afterdepolarizations, and fibrillation. *Cardiovasc Res* **99**, 215–224.

Klein G, Schroder F, Vogler D, Schaefer A, Haverich A, Schieffer B, Korte T, & Drexler H (2003). Increased open probability of single cardiac L-type calcium channels in patients with chronic atrial fibrillation: role of phosphatase 2A. *Cardiovasc Res* **59**, 37–45.

Li GR & Nattel S (1997). Properties of human atrial I_{Ca} at physiological temperatures and relevance to action potential. *Am J Physiol Heart Circ Physiol* **272**, H227–H235.

Madhvani RV, Angelini M, Xie Y, Pantazis A, Suriany S, Borgstrom NP, Garfinkel A, Qu Z, Weiss JN, & Olcese R (2015). Targeting the late component of the cardiac L-type Ca^{2+} current to suppress early afterdepolarizations. *J Gen Physiol* **145**, 395–404.

Madhvani RV, Xie Y, Pantazis A, Garfinkel A, Qu Z, Weiss JN, & Olcese R (2011). Shaping a new Ca^{2+} conductance to suppress early afterdepolarizations in cardiac myocytes. *J Physiol* **589**, 6081–6092.

Neher E (1992). Correction for liquid junction potentials in patch clamp experiments. *Methods Enzymol* **207**, 123–131.

Nguyen TP, Xie Y, Garfinkel A, Qu Z, & Weiss JN (2012). Arrhythmogenic consequences of myofibroblast-myocyte coupling. *Cardiovasc Res* **93**, 242–251.

Numata A, Miyauchi Y, Ono N, Fishbein MC, Mandel WJ, Lin SF, Weiss JN, Chen PS, & Karagueuzian HS (2012). Spontaneous atrial fibrillation initiated by tyramine in canine atria with increased sympathetic nerve sprouting. *J Cardiovasc Electrophysiol* **23**, 415–422.

Nygren A, Fiset C, Firek L, Clark JW, Lindblad DS, Clark RB, & Giles WR (1998). Mathematical model of an adult human atrial cell: the role of K^+ currents in repolarization. *Circ Res* **82**, 63–81.

Ortega FA, Grandi E, Krogh-Madsen T, & Christini DJ (2018). Applications of dynamic clamp to cardiac arrhythmia research: role in drug target discovery and safety pharmacology testing. *Front Physiol* **8**, 1099.

Prinz AA, Abbott LF, & Marder E (2004). The dynamic clamp comes of age. *Trends Neurosci* **27**, 218–224.

Qu Z, Xie LH, Olcese R, Karagueuzian HS, Chen PS, Garfinkel A, & Weiss JN (2013). Early afterdepolarizations in cardiac myocytes: beyond reduced repolarization reserve. *Cardiovasc Res* **99**, 6–15.

Sato D, Xie L-H, Sovari AA, Tran DX, Morita N, Xie F, Karagueuzian H, Garfinkel A, Weiss JN, & Qu Z (2009). Synchronization of chaotic early afterdepolarizations in the genesis of cardiac arrhythmias. *Proc Natl Acad Sci U S A* **106**, 2983–2988.

Stambler BS, Fenelon G, Shepard RK, Clemo HF, & Guiraudon CM (2003). Characterization of sustained atrial tachycardia in dogs with rapid ventricular pacing-induced heart failure. *J Cardiovasc Electrophysiol* **14**, 499–507.

Watanabe I, Okumura Y, Nagashima K, Ohkubo K, Ashino S, Kofune M, Ohya T, & Hirayama A (2010). Electrical remodeling in fibrillating canine atrium: action potential alternans during rapid atrial pacing and late phase 3 early afterdepolarization after cessation of rapid atrial pacing. *Int Heart J* **51**, 354–358.

Weiss JN, Garfinkel A, Karagueuzian HS, Chen PS, & Qu Z (2010). Early afterdepolarizations and cardiac arrhythmias. *Heart Rhythm* **7**, 1891–1899.

Wilders R (2006). Dynamic clamp: a powerful tool in cardiac electrophysiology. *J Physiol* **576**, 349–359.

Wit AL & Boyden PA (2007). Triggered activity and atrial fibrillation. *Heart Rhythm* **4**, S17–S23.

Workman AJ (2010). Cardiac adrenergic control and atrial fibrillation. *Naunyn-Schmiedebergs Arch Pharmacol* **381**, 235–249.

Workman AJ, Kane KA, & Rankin AC (2001). The contribution of ionic currents to changes in refractoriness of human atrial myocytes associated with chronic atrial fibrillation. *Cardiovasc Res* **52**, 226–235.

Workman AJ, Kane KA, & Rankin AC (2008). Cellular bases for human atrial fibrillation. *Heart Rhythm* **5**, S1–S6.

Workman AJ, Kane KA, & Rankin AC. (2000). Rate-dependency of action potential duration and refractoriness in isolated myocytes from the rabbit AV node and atrium. *J Mol Cell Cardiol* **32**, 1525–1537.

Workman AJ, Marshall GE, Rankin AC, Smith GL, & Dempster J (2012). Transient outward K^+ current reduction prolongs action potentials and promotes afterdepolarisations: a dynamic-clamp study in human and rabbit cardiac atrial myocytes. *J Physiol* **590**, 4289–4305.

Workman AJ, Smith GL, & Rankin AC (2011). Mechanisms of termination and prevention of atrial fibrillation by drug therapy. *Pharmacol Ther* **131**, 221–241.

Yan G-X, Wu Y, Liu T, Wang J, Marinchak RA, & Kowey PR (2001). Phase 2 early afterdepolarization as a trigger of polymorphic ventricular tachycardia in acquired long-QT syndrome. Direct evidence from intracellular recordings in the intact left ventricular wall. *Circulation* **103**, 2851–2856.

Yeh YH, Wakili R, Qi XY, Chartier D, Boknik P, Kaab S, Ravens U, Coutu P, Dobrev D, & Nattel S (2008). Calcium-handling abnormalities underlying atrial arrhythmogenesis and contractile dysfunction in dogs with congestive heart failure. *Circ Arrhythmia Electrophysiol* **1**, 93–102.

Zhao Z, Wen H, Fefelova N, Allen C, Baba A, Matsuda T, & Xie L-H (2012). Revisiting the ionic mechanisms of early afterdepolarizations in cardiomyocytes: predominant by Ca waves or Ca currents? *Am J Physiol Heart Circ Physiol* **302**, H1636–H1644.

Additional information

Competing interests

The authors declare that they have no competing interests.

Author contributions

to be accountable for all aspects of the work in ensuring that questions related to the accuracy or integrity of any part of the work are appropriately investigated and resolved, and all persons designated as authors qualify for authorship, and all those who qualify for authorship are listed.